Hardware developments and commissioning of the imaging heavy ion beam probe at ASDEX Upgrade [*]

May 7, 2021

G. Birkenmeier[1,2], J. Galdon-Quiroga[1], V. Olevskaia[2], P. Oyola[3], J.J. Toledo-Garrido[4], K. Bald[1], M. Sochor[1], G. Anda[5], S. Zoletnik[5], A. Herrmann[1], V. Rohde[1], M. Teschke[1], L. Giannone[1], T. Lunt[1], E. Viezzer[3,4], M. Garcia-Munoz[3,4], and the ASDEX Upgrade team[6]

[1]Max Planck Institute for Plasma Physics, Boltzmannstr. 2, 85748 Garching

[2]Physics Department E28, Technical University Munich, James-Franck-Str. 1, 85748 Garching, Germany

[3]Department of Atomic, Molecular and Nuclear Physics, Universidad de Sevilla, 41012 Seville, Spain

[4]Centro Nacional de Aceleradores (CNA), Universidad de Sevilla, 41092 Seville, Spain

[5]Fusion Technology Department, Centre for Energy Research, Budapest, Hungary

[6]See author list in H. Meyer et al., Nucl. Fusion **59** ,112014 (2019)

Abstract

The imaging heavy ion beam probe (i-HIBP) is a new diagnostic concept realized at the tokamak ASDEX Upgrade (AUG) in order to obtain two-dimensional information about the density, the magnetic field and the electrostatic potential at the plasma edge. Although the two main components of the i-HIBP, an alkali beam based injector and a scintillator based detector, involve well-developed technologies, further developments were necessary to realize the i-HIBP at AUG. In dedicated laboratory tests, a new type of cesium source was characterized and the neutralization efficiency and properties of the primary cesium beam were found to be similar to alkali beams made of lighter elements. The use of cesium had also impact on the choice of the scintillator material, which was experimentally investigated in terms of photon yield, energy dependence and degradation revealing significant differences under irradiation with cesium ions compared to irradiation with hydrogenic beams. Due to constrictions of the AUG experiment setup, the high voltage components, the in-vessel shutter technology and the maintenance capabilities of the i-HIBP required new developments for the commissioning of the diagnostic.

1   Introduction

At the boundary of magnetically confined fusion plasmas around the last closed flux surface (LCFS) a wide variety of phenomena exist in different plasma regimes due to the presence of a strong pressure gradient and the special topology of the magnetic field including the transition from open to closed field lines. These include magneto-hydrodynamic instabilites like edge localized modes [1], which are sought to be avoided in reactor relevant regimes [2], beneficial flows generated by neoclassical [3] or turbulent effects [4], or bursty events like blobs [5], limit-cycle oscillations [6] and intermittent density fluctuations [7] for which the role in a future reactor is not clear yet. In order to understand these phenomena and their role for future reactors in more detail, a proper experimental characterization by plasma edge diagnostics with high temporal and spatial resolution is required.

Heavy ion beam diagnostics were very successfully used to measure density, magnetic field and electrostatic potential perturbations at different plasma devices using *out-vessel* detectors [8, 9, 10, 11]. A new approach, which tries to access the same quantities at the plasma edge by means of an *in-vessel* detector, is the imaging heavy ion beam probe (i-HIBP) [12, 13], which was commissioned at ASDEX Upgrade (AUG) in 2020. Similar to the atomic beam probe concept at the COMPASS tokamak [14, 15], an alkali beam injector specialized for fusion applications [16] is used for the i-HIBP in order to inject a high energetic neutral beam into the AUG plasma. This neutral primary beam, typically cesium at an energy of up to 70 keV, is ionized in the plasma, where a fan of singly charged cesium beams is created. These secondary beams perform an almost circular trajectory due to the Lorentz force in the tokamak magnetic field and gyrate into the limiter shadow where they are detected by a scintillator-based detector.
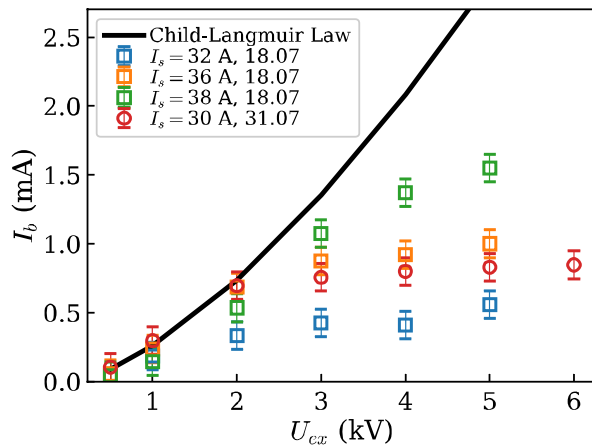
Figure 1: Extracted beam current I_b vs. extraction voltage, U_{ex}. For low extraction voltages, the measured current (symbols) follows the Child-Langmuir law (black line) and saturates for higher voltages due to the heating limit of the thermionic extraction.

The fan of secondary beams create a linearly shaped pattern on the scintillator, the so called scintillator strike line, detected by a high speed camera. The strike line contains information from different radial positions of the plasma, and if an aperture plate with multiple pinholes is placed into the primary beam line, multiple strike lines are detectable which contain additional information from poloidally separated regions. Intensity perturbations of the strikeline are related to density perturbations (and to a lower degree to temperature perturbations) and (local) displacements of the strikeline allow to determine magnetic field and electrostatic potential perturbations. A detailed description of the measurement principle is given in Refs. [12, 13].

Although the main components of the i-HIBP are based on well-developed technologies, namely an alkali beam injector as routinely used for beam emission spectroscopy applications [16] and a scintillator-based detector similar to fast ion loss detectors [17], a few further developments were necessary to apply the i-HIBP technique at AUG. The requirement to use cesium for the probing beam made the development of new ion source materials necessary and required to study the scintillator properties under cesium irradiation, since lighter elements are normally used in the context of these technologies. Laboratory experiments were employed to investigate these aspects as described in section 2. The design of the injector geometry and support structures is presented in section 3, which was optimized for the given space restrictions in the AUG experimental setup, especially in terms of maintenance capabilities. Section 4 deals with the in-vessel components and the most recent status of the detector head. A summary and an outlook of the prospects of the i-HIBP at AUG are given section 5.

2 Cesium beam and scintillator properties

In order to be able to detect a measurable ion flux on the scintillator of a few mA/m^2, the incident primary beam must deliver an equivalent current of more than 3 A/m^2 on a circular spot of about 1 mm in diameter in the plasma [13]. This high neutral beam intensities have reliably been realized despite the harsh environments of a fusion experiment by alkali beam injectors [16]. The alkali beam injector design, which is used for the i-HIBP diagnostic at AUG, was successfully applied at several fusion experiments in order to create neutral beams of lithium and sodium by thermionic extraction predominantly for beam emission spectroscopy applications [18, 19, 20, 21]. It consists of an ion source, accelerator electrodes, ion optics for beam focussing, two pairs of deflection plates for vertical and horizontal beam steering, a low-loss neutralizer for beam neutralization and a set of Faraday cups and cameras for beam diagnosis [16]. In contrast to the alkali beam diagnostics at other fusion experiments, the i-HIBP at AUG requires the use of heavier alkali elements in order to get a sufficiently large Larmor radius of the detected ions at the given beam energy, so that they propagate far enough into the limiter shadow where the scintillator detector is located. This requirement is only fulfilled for cesium at 55 kV or rubidium at 70 kV for the typical AUG magnetic field of 2.5 T and made the development of new sources necessary, since only lighter alkali ions (Li, Na, K) were routinely used in this type of injector so far. In this article, we focus on the description and investigation of a cesium beam.

The cesium source is a $Cs_2O \cdot Al_2O_3 \cdot 4SiO_2$ disk of a diameter of 14 mm manufactured by Entimel Kft. By thermionic extraction, a beam current up to 1.5 mA can be extracted from this emitter material when it is electrically heated up to 1250° C. This beam current is significantly lower than usually extractable from lithium or sodium emitters of the same diameter [16]. As shown in Fig. 1, the measured extracted beam current I_b (symbols) is space charge limited at lower extraction voltages U_{ex} and follows approximately the Child-Langmuir law (black line). For higher extraction voltages, the beam current saturates on a level which is given by the temperature limit of the emission material. In this saturated regime, the ion diffusion inside the bulk material of the emitter is too low, so that the current cannot rise even if a higher extraction voltage is applied. If a higher source heating, quantified by the heating current I_s, is applied, higher extracted currents can be achieved. This effect is clearly seen for $U_{ex} = 5$ kV measured on 18th July 2019, where the extracted current almost triples when the heating current I_s is increased from 32 A corresponding to 119 W (blue) to 38 A corresponding to 142 W (green). The cesium emitter showed a conditioning effect manifesting in comparably high extracted beam currents when the measurement was repeated again after a few days of regular beam operation, although the heating power was much lower (112 W, red). Despite the cesium beam is inferior to beams of other alkali elements in terms of maximum extracted currents, the design goal of a beam current $I_b > 1$ mA corresponding to an injected beam current density of $j_b > 3$ mA/m^2 after collimation down to the desired spot size was achieved. Other properties like focussing, divergence,

control and the ability to be neutralized by a sodium vapor cell is identical to lithium or sodium beams as described in Ref. [16] and was verified in dedicated laboratory tests.
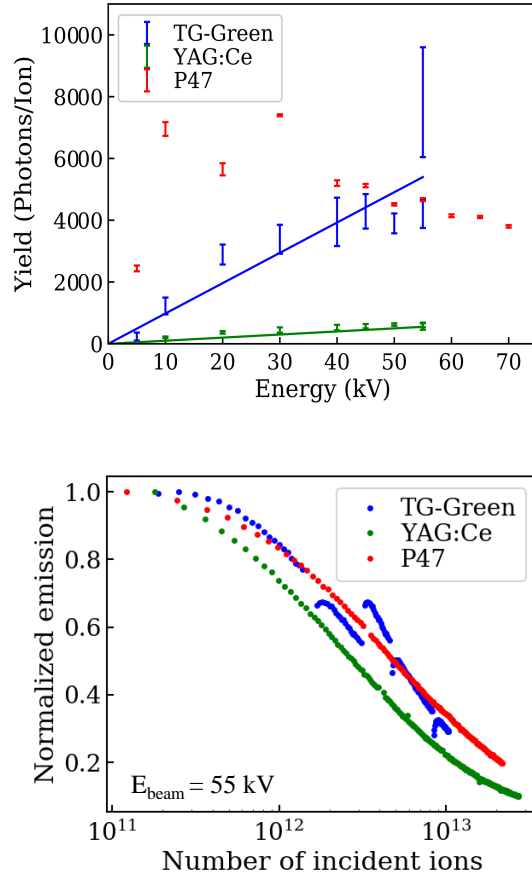

Figure 2: Photon yield depending on energy (top) and degradation of the photon yield vs. accumulated Cs ion flux (bottom) for three different scintillator materials as determined in dedicated laboratory tests for the identification of a suitable i-HIBP scinitillator material.

The choice of cesium for the probing beam necessitated investigations of the compatibility of cesium with established scintillator materials as broadly used in fast ion loss detectors on different fusion experiments [17, 22, 23, 24, 25]. This is because the scintillators are well known to work with light elements (H, D, T, He) [26] but their properties under heavy ion irradiation is less well documented. In dedicated laboratory tests, we determined the light yield, the energy

Side View of i-HIBP Setup

Rail system

Plasma

Ion beam

Neutral
primary beam

Neutralizer

Ion source and ion
optics

Vacuum
vessel

Detector head

Deflection plates

Operation Position (Top View)

Maintenance Position (Top View)

Injector

Plasma
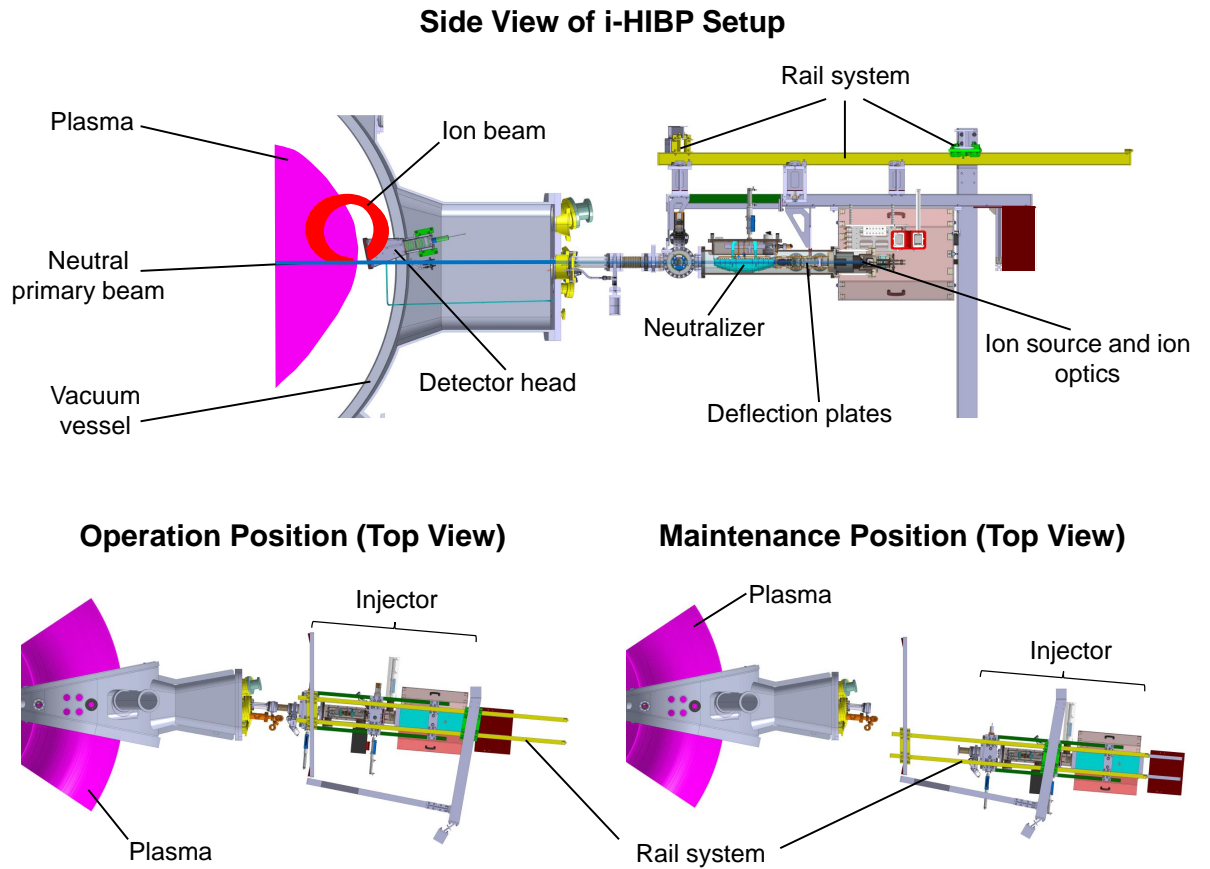
Plasma

Injector

Plasma

Rail system

Figure 3: Side view of the i-HIBP setup at AUG (top). During operation, the
i-HIBP injector is connected to the AUG vacuum vessel (bottom left). During
maintenance intervals, the injector can be disconnected from the vacuum vessel
in order to improve the accessibility for other diagnostics (bottom right). By
means of two coupled rail systems and a spindle, the whole injector can be
displaced along three axes.

dependence and degradation of different scintillator materials under cesium irradiation. A detailed description of the experimental setup and the results are published elsewhere [27]. The photon yield i.e. the number of photons that are emitted from the scintillator per incident ion depends on the energy of the incident ions and should be maximized in order to obtain a signal intensity as high as possible. Fig. 2, top, shows the photon yield of three scintillator materials: TG-Green ($SrGa_2S_4$:Eu^{2+}), YAG:Ce ($Y_3Al_5O_{12}$:Ce^{3+}) and P47 (Y_2SiO_5:Ce^{3+}). TG-Green and YAG:Ce exhibit a desired linear relation between yield and incident ion energy, while P47 does not. The maximum yield of TG-Green is in the order of 6000 photons per ion. This is in the same order of magnitude as the estimated yield for TG-Green irradiated with deuterium [28], and demonstrates the capability of a scintillator to amplify signals. This way an ion current of 1 nA typically achieved for line-averaged plasma densities of $2.0 \cdot 10^{19}$ m^{-3}, that reaches the scintillator plate in an area of 1 mm^2 and that would be difficult to be electrically measured in the tokamak environment, is translated into $3.72 \cdot 10^{13}$ photons per second, which is a significant light level easily detectable with an appropriate optics and a high speed camera.

This signal intensity, however, has to be compared with the background light level on the scintillator from reflections of visible light and scintillator luminescence induced by high energetic ions, high energetic neutrals or X-rays. Light reflections are minimized by a black coating inside the detector head, and the fact that the scintillator is facing away from the plasma enables only very high energetic ions with very large Larmor radii to reach the scintillator. Particle tracer simulations show, that significant ion fluxes can only be expected at the very top of the scintillator, while the bottom part, where we expect the highest signal intensities from the Cs beam [13], should be free from this background noise. This is confirmed in first measurements with the detector head in more than 60 plasma discharges without injection of Cs, in which we found in L-mode only a very faint and homogenous background light from the scintillator correlated with the bolometrically determined total plasma radiation. In H-mode, however, the background is much higher during the ejection of edge localized modes, which reach far into the limiter shadow and emit light and neutrals illuminating the scintillator significantly. In order to be able to measure during these time periods, we will have to use fast beam chopping up to 250 kHz for background subtraction during beam-off phases as already implemented in the hardware.

As shown in Fig. 2, bottom, the photon yield degrades exponentially in a wide range of fluence for all scintillator materials and reaches half of the yield after an accumulated ion flux of about $5 \cdot 10^{12}$ ions. The non-monotonic dependence of the degradation curve of TG-Green (blue curve) is an experimental artefact resulting from focussing problems during the beam extraction phase. The degradation is much stronger for cesium than for lighter elements, and is related to the fact that heavy ions deposit their kinetic energy in a shallower layer of the scintillator material leading to a more concentrated damage than for lighter elements of the same energy [27, 28]. The degradation of the photon yield of the scintillator imposes severe limitations on the operation of the

7

i-HIBP detector: after about 100 AUG discharges the light yield is halved as can be estimated from typical expected ion fluxes during i-HIBP operations, if no countermeasures are taken. Thus, the scintillator detector must only be used in dedicated plasma scenarios, and the point of ion impact on the scintillator must be varied from time to time. Additional degradation effects due to neutrals or neutrons are not expected, since the operation of TG-Green scintillator screens in fast ion loss detectors for more than ten years of operation in AUG have not shown any significant degradation.

Overall, the TG-Green scintillator material showed a desirable performance under cesium irradiation, and has the additional advantage of an emission peak around 550 nm, which is favourable in terms of transmission through optical components compared to P47, which has its emission peak at around 400 nm. Therefore, TG-Green was selected for the i-HIBP detector at AUG.

3 Injector and out-vessel setup

Although the principle design of the alkali beam injector was already available from injectors at other machines [16], several design aspects had to be modified. First, the high voltage (HV) components like a transformer, resistors and the HV voltage cage around the acceleration area could not be supported by an injector table from below but had to be mounted from the top in order to fit into the experiment environment of AUG in sector 13. Secondly, in order to avoid that the comparably large i-HIBP injector blocks many other diagnostics, it was mounted on two coupled rail systems, which allow to move the injector in radial and toroidal direction, and a spindle in order to move the injector up and down. A comparison of the operation position and the parking position during maintenance intervals is shown as a CAD drawing in Fig. 3. This way, access to other diagnostic ports is enabled or facilitated, which is necessary during maintenance periods.

4 In-vessel components

The in-vessel detector head is placed at the outer midplane of AUG sector 13 and houses the 6 cm × 16 cm scintillator plate covered with TG-Green powder, the lens system, a lamp, a thermo couple and a current measurement at the scintillator plate. A schematic CAD drawing of the detector head is shown in Fig. 4. The secondary cesium beams enter the head through a rectangular opening from the top (see also Fig. 4 in Ref. [13]). The light emitted by the scintillator is collected by a lens system consisting of six lenses and a diaphragm that guide the image of the scintillator into an image guide transferring the image to the vacuum window of an AUG port behind which a camera is placed. The image guide consists of 700×1700 fibres with a diameter of 10 μm, and sets the spatial resolution of the system to resolve structures of about 100 μm on the scintillator. A scintillator shutter with a drive of 5 cm is mounted in
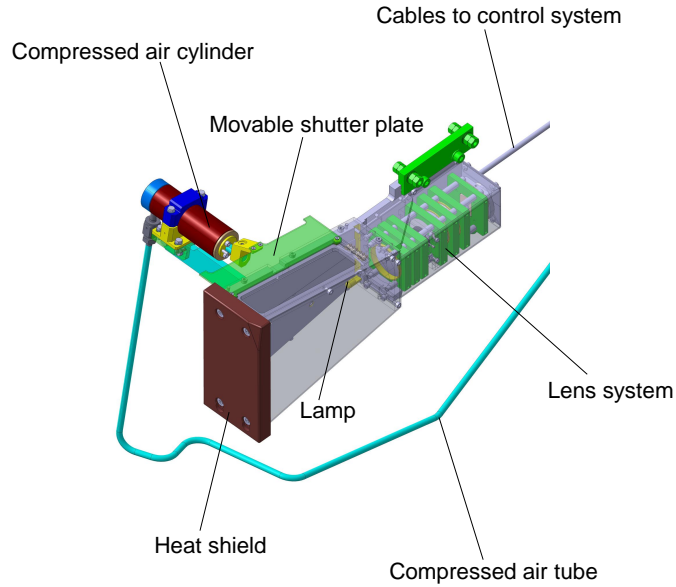
Figure 4: CAD drawing of the in-vessel detector head of the i-HIBP. The scintillator plate (not visible) facing the lens system is placed behind the heat shield.

order to protect the scintillator from damage or coating by undesired elements especially during glow discharges or boronization for wall conditioning. This shutter is driven by compressed air in order to allow opening and closing on demand without involving in-vessel electronics. A thermocouple monitors the temperature of the scintillator for safety purposes, and a current measurement at the scintillator plate can be used to determine the integrated ion flux onto the scintillator. A lamp is installed to monitor the transmission of the optical system, which can significantly degrade due to neutron radiation from the plasma affecting the image guide in particular. As known from similar image guides operated in other places of the AUG vessel, the transmission can be reduced by a factor of 100 due to neutron damage during one AUG measurement campaign. Thus, the i-HIBP image guide must be taken out of the vacuum vessel after every campaign in order to bake it at about 200 degree Celsius to regain the initial transmission of the image guide. A tungsten-coated graphite plate serves as heat shield of the detector head, which is placed into the limiter shadow having a distance of minimum 2 cm to the local far scrape-off layer plasma.

5   Summary and Outlook

The main components of the i-HIBP diagnostic were tested in dedicated laboratory experiments, and the key design criteria were verified. This includes

a stable operation of a neutral cesium beam up to 70 keV, a beam current of more than 1 mA, and a neutralization efficiency by the sodium vapor cell of about 80%. Based on the scintillator material investigations, the TG-Green scintillator with a photon yield of about 6000 photons per ion was selected and manufactured.

The installation of the full i-HIBP system inside and outside the vacuum vessel of AUG was finished at the end of 2019. Since then, the i-HIBP was gradually commissioned until the scheduled end of the AUG plasma operation phase in July 2020. Besides the anticipated technical problems of i-HIBP components like malfunctioning of electronics in the tokamak field or during disruptions, the commissioning was mainly hampered by two unexpected issues. First, the appearance of strong sparking of HV components at 55 kV, which did not appear during the laboratory tests, limited the accessible HV range. This is probably due to more powerful and self-sustaining sparks induced by inductivities ("inductive kickback") of the HV cables ranging 40 m between the HV generators and the torus hall, which were not part of the system during the laboratory tests. Changes in the HV setup and hardening of selected HV components will avoid this in the future. Second, an HV insulator between extractor and emitter electrode made of PEEK (polyether ether ketone) became conductive at higher temperatures. As a consequence, a cesium beam could be extracted only at low source heating, but not at relevant temperatures, which are needed to heat the ion source at the operational point. Most probably, the PEEK became conductive due to chemical interaction with the hot sodium present in the beam line generated in the neutralizer cell. Therefore, the insulator is now replaced by aluminium oxide which is more chemically inert in respect of sodium.

With these modifications, the i-HIBP is fully operational and first signals are expected during the AUG campaign 2021.

References

[1] H. Zohm et al., Plasma Phys. Control. Fusion 38 (1996) 105-128.

[2] E. Viezzer et al., Nucl. Fusion 58 (2018), 115002, doi:10.1088/1741-4326/aac222

[3] E. Viezzer et al., Nucl. Fusion 54 (2014) 012003

[4] G.D. Conway et al., Plasma Phys. Control. Fusion 47 (2005) 1165

[5] D.A. D'Ippolito et al., Phys. Plasmas 18 (2011) 060501

[6] G. Birkenmeier et al., Nucl. Fusion 56 (2016) 086009

[7] T. Happel et al., Plasma Physics and Controlled Fusion 59, (2017) 014004, doi:10.1088/0741-3335/59/1/014004

[8] D.R. Demers et. al, Phys. Plasmas 8 (2001) 1278, https://doi.org/10.1063/1.1355674

[9] R. Sharma et al., Fusion Engineering and Design, Volume 160, 2020, 112016, ISSN 0920-3796, https://doi.org/10.1016/j.fusengdes.2020.112016.

[10] A.V. Melnikov et al., Nucl. Fusion 50 (2010) 084023 (11pp) doi:10.1088/0029-5515/50/8/084023

[11] T. Kobayashi et al., Phys. Rev. Lett. 111 (2013), https://doi.org/10.1103/physrevlett.111.035002

[12] J. Galdon-Quiroga et al., Journal of Instr. 12 (2017) C08023

[13] G. Birkenmeier et al., JINST 14 (2019) C10030

[14] M. Berta et al., Fus. Eng. Des. 88 (2013) 2875

[15] P. Hacek et al., Review of Scientific Instruments 89, 113506 (2018); https://doi.org/10.1063/1.5044529

[16] G. Anda et al., Rev. Sci. Instr. 89 (2018) 013503

[17] M. Garcia-Munoz et al., Rev. Sci. Instrum. 80 (2009) 053503

[18] G. Anda et al., Fusion Engineering and Design 108 (2016) 1-6

[19] G. Anda et al., Fusion Engineering and Design 146 (2019) 1814-1819

[20] M. Lampert et al., Review of Scientific Instruments 86, 073501 (2015); https://doi.org/10.1063/1.4923251

[21] Y.F. Wang et al., Fusion engineering and design 144C (2019): 133-140

[22] R.K. Fisher et al., Rev. Sci. Instrum. 81 (2010) 10D307

[23] J. Kim et al., Rev. Sci. Instrum. 83 (2012) 10D305

[24] S. Baeumel et al., Review of Scientific Instruments 75 (2004) 3563

[25] M. Rodriguez-Ramos et al., Nuclear Instruments and Methods in Physics Research B 403 (2017) 7-12 http://dx.doi.org/10.1016/j.nimb.2017.04.084

[26] M.C. Jimenez-Ramos et al., Nuclear Instruments and Methods in Physics Research B 332 (2014) 216-219, https://doi.org/10.1016/j.nimb.2014.02.064

[27] J.J. Toledo-Garrido et al., in preparation

[28] M. Rodriguez-Ramos et al., Plasma Phys. Control. Fusion 59 (2017) 105009, https://doi.org/10.1088/1361-6587/aa7e5f